HHS Public Access

Author manuscript

Magn Reson Med. Author manuscript; available in PMC 2017 September 01.

Published in final edited form as:

Magn Reson Med. 2016 September ; 76(3): 897–904. doi:10.1002/mrm.25979.

Variable flip angle 3D-GRASE for high resolution fMRI at 7 T

Valentin G. Kemper[1,2], **Federico De Martino**[1,2,3], **Essa Yacoub**[3], and **Rainer Goebel**[1,2]

[1]Department of Cognitive Neuroscience, Faculty of Psychology and Neuroscience, Maastricht University, Oxfordlaan 55, 6200 MD Maastricht, The Netherlands [2]Maastricht Brain Imaging Center, Maastricht University, Oxfordlaan 55, 6200 MD Maastricht, The Netherlands [3]Center for Magnetic Resonance Research, University of Minnesota Medical School, 2021 Sixth Street SE, Minneapolis, MN 55455, United States of America

Abstract

Purpose—To evaluate the use of variable flip angle refocusing pulse trains in single-shot 3D gradient and spin-echo (3D-GRASE) in order to reduce blurring and increase the spatial coverage for high spatial resolution T_2-weighted functional MRI at 7 T.

Methods—Variable flip angle refocusing schemes in 3D-GRASE were calculated based on extended phase graph theory. The blurring along the slice (partition) direction was evaluated in simulations, as well as phantom and in-vivo experiments. Further, temporal stability and functional sensitivity at 0.8 mm isotropic resolution were assessed.

Results—Variable flip angle refocusing schemes yielded significantly reduced blurring compared to conventional refocusing schemes, with the full width at half maximum being about 30-40 % narrower. Simultaneously, spatial coverage could be increased by 80 %. The temporal signal-to-noise ratio was slightly reduced, but functional sensitivity was largely maintained due to increased functional contrast in the variable flip angle acquisitions. Signal-to-noise ratio and functional sensitivity were reduced more strongly in areas with insufficient RF transmission indicating higher sensitivity to experimental imperfections.

Conclusion—Variable flip angle refocusing schemes increase usability of 3D-GRASE for high-resolution fMRI by reducing blurring and allowing increased spatial coverage.

Keywords

3D-GRASE; high-resolution fMRI; variable flip angle; T2 weighted fMRI; point-spread function; 7 T

Introduction

Simulations and experiments have shown that at ultra-high field (i.e. 7 T and above) the T_2-weighted blood oxygen level dependent (BOLD) signal is more specific to the site of neuronal activity than T_2*-weighted BOLD (at either high or low field), because T_2-

Corresponding author: Valentin G. Kemper (valentin.kemper@maastrichtuniversity.nl), Address: P.O. Box 616, 6200 MD Maastricht, The Netherlands, Phone: +31 43 38 84035, Fax: +31 43 38 84125.

weighted BOLD is less sensitive to large draining veins (1-3). However, regardless of the increased signal to noise ratio available at higher field (4,5), purely T_2-weighted acquisition strategies (6-11) have been hindered in high-resolution applications by their long acquisition time, lower sensitivity, and/or the high specific absorption rate (SAR). The temporal efficiency and (relative) SAR parsimony of spin-echo echo planar imaging (SE-EPI, (12)) partly alleviate these issues. However, EPI readouts introduce T_2* contrast, depending on the echo train length, compromising purely T_2-weighted contrast (13). To counteract this, outer-volume suppression (14,15), inner-volume selection by orthogonal radio-frequency (RF) pulse plain prescriptions (16), and segmented EPI trains have been used (3).

In the study of human brain function, the successful use of the latter two methods has been showcased by a single-slice 2D SE-EPI with anisotropic resolution (17,18). Despite this success, the method did not find applicability outside a flat piece of cortex in primary visual areas. Extending this approach, to overcome the limitation of acquiring a single anisotropic slice, 3D inner-volume gradient echo and spin echo (3D-GRASE, (19,20)) has been proposed. 3D-GRASE acquires a full 3D volume after a single excitation pulse by sampling k-space with a combination of EPI echo trains and multiple spin-echoes. The refocusing RF pulses select a perpendicular slab achieving inner-volume selection. We have recently shown that 3D-GRASE is functionally more specific and more sensitive than 2D SE-EPI with a large field of view (FoV) (21), however, blurring along the secondary phase-encoding direction (partition direction) and the small FoV of 3D-GRASE still limit its usability. In particular, the FoV of 3D-GRASE cannot easily be extended as doing so introduces T_2 decay induced blurring (additionally T_2* blurring and T_2* functional contrast when increasing the in-plane FoV). To alleviate the blurring introduced by T_2 decay, the signal strength would have to be sustained throughout the echo train (22). This can be achieved by variable flip angle refocusing RF pulse trains, which introduce alternative signal pathways (stimulated echoes and additional primary spin-echoes of various pairs of RF pulses). They are designed based on extended phase graph theory (23) and are routinely employed in T_2-weighted turbo spin echo (RARE/FSE/TSE) (24) structural imaging (known as SPACE, VISTA or CUBE) (25,26).

In this proof-of-concept study, we apply VFA refocusing trains in high spatial resolution single-shot 3D-GRASE. We validate the method in phantom acquisitions and demonstrate two cases of successful in-vivo application to (a) reduce the blurring and to (b) simultaneously reduce blurring and extend the imaging FoV. Accelerated imaging (27,28) as a potential alternative to increase the in-plane FoV is also explored.

Methods

All measurements were performed on a 7T Magnetom Siemens scanner equipped with a body gradient system (70 mT/m maximum amplitude, 200 mT/m/s maximum slew rate). A 32-channel phased-array head coil (Nova Medical, Wilmington, MA, USA) was used in phantom measurements and a 16-channel phased array surface coil (Live Services, Minneapolis, MN, USA) covering the posterior part of the subjects' heads was used for in-vivo experiments. Eight healthy volunteers (5 female; mean age 27 ± 4 years) were scanned after giving informed written consent and in compliance with the local ethical board. One

subject (S 5) was excluded from functional analyses, because she reported sleepiness after the measurements. Second order automatic static field shim routines were applied and refined manually to reach good static field homogeneity (in-vivo: Larmor frequency full width at half maximum ≤ 45 Hz, $T_2^* = 15.1 \pm 1.4$ ms). RF transmission voltage was adjusted based on a pre-saturation based B_1-mapping sequence provided by the scanner vendor. A small region of interest in the center of the imaging volume was used to determine the correct voltage.

Variable flip angle refocusing design

The variable flip angle pulse trains were calculated offline using MATLAB (The MATHWORKS Inc., Natick, MA, USA). It was assumed that the signal evolution along the partition encoding direction could be treated separately from the decay due to T_2 and T_2', which affects the phase encoding direction. Further, it was assumed that the Carr-Purcell-Meiboom-Gill (CPMG) condition was met for the central spin-echoes of the EPI echo trains. An exponential target signal decay was calculated taking into account TE, number of slices (also accounting for k-space truncation), partial Fourier (assuming zero-filling), the desired maximum blurring along the partition-direction, and the relaxation properties of the target tissue (T_2 = 40 ms, T_1 = 400 ms for agar phantom, T_2 = 50 ms, T_1 = 1800 ms for gray matter). The calculation of the VFA echo train for a given target signal shape was then done as suggested in (25) based on (23,29). Finally, the flip angles of the last third of the echo train were raised quadratically in the in-vivo scans to maximize the signal intensity. The last refocusing flip angle was raised to the maximum of the echo train rather than to 180° that would otherwise require longer refocusing pulses. Care was taken that the resulting signal intensities of the alternated last refocusing flip angles were all higher than in the exponential decay to ensure blurring would not become stronger due to the alternation.

Point-spread function measurements

Global point-spread function measurements were performed by acquiring non-Fourier-encoded images (21). After four volume acquisitions in order to reach a steady state, the phase-encoding gradients in the in-plane and partition directions were switched off for the fifth repetition. Instead of sampling a full k-space, the k-space center line was acquired repeatedly in every read-out, modulated by the modulation transfer function (MTF). The resultant data can be reconstructed in the reconstruction pipeline exhibiting the anisotropic image point-spread function (PSF), reflecting effects of the acquisition (i.e. signal modulation due to T_2 and T_2^* decay) and the reconstruction (i.e. filtering) (30-32). The ideal case of a homogeneous MTF would result in a sharply peaked intensity distribution along the non-encoded directions. However, in practice, the obtained PSF has a finite width. In order to characterize the PSF, we computed the full width at half maximum (FWHM) by interpolating the magnitude of the PSF using a spline interpolation. This approach was chosen rather than a Gaussian fit (21) because it characterized the different peak shapes of the VFA acquisitions better.

Phantom measurements

A spherical agar phantom was used to test the VFA approach systematically in a wide range of parameter combinations. VFA pulse trains were calculated for each of the 4×3×3

combinations of 1) FWHM of PSFs of 2, 2.5, 3, and 4 pixels, 2) coverage of 10, 16, and 20 slices, and 3) partial Fourier acquisition of 5/8, 7/8, and 8/8 (except Partial Fourier 5/8 at 2 pixel FWHM was not performed with 10 slices because it would require a constant MTF). Other imaging parameters were as in the in-vivo REF measurement (see below).

In-vivo measurements

Four different 3D-GRASE measurements were acquired with each subject: 1) a conventional 3D-GRASE acquisition with nominal 180° refocusing pulses (REF); 2) a variable flip angle acquisition with otherwise same protocol as REF with reduced blurring (VFA1); 3) a variable flip angle acquisition to extend the FoV in partition-direction and with reduced blurring (VFA2); 4) the same protocol as REF, except GRAPPA factor 2 and doubled FoV in in-plane phase encoding direction (R2). TE in VFA1 and VFA2 could be slightly reduced compared to REF because of the shorter RF pulse lengths required for the smaller flip angles. See Table 1 for additional imaging parameters. The nominal refocusing flip angles used for VFA1 were (109°-63°-62°-63°-75°-109°), and for VFA2 (90°-49°-45°-43°-43°-43°-42°-43°-46°-51°-58°-67°-77°-90°). All acquisitions used 90° nominal excitation flip angles, linear phase ordering in in-plane direction, and centric ordering of the partition direction.

A T_1-weighted MPRAGE sequence (isotropic resolution of 0.6 mm; TR = 3100 ms; TI = 1500 ms; TE = 2.52 ms; Flip angle = 5°; GRAPPA acceleration factor = 3; FoV = 230×230×154 mm^3; duration 8:49 min.) was used to acquire structural images for anatomical reference. Additionally, a proton density weighted MPRAGE with identical imaging parameters except without an inversion module (and: TR=1440 ms, duration 4:06 min.) was acquired to alleviate inhomogeneities across the FoV in post-processing by dividing the T_1-weighted image by the proton density weighted images (33).

Visual stimulation paradigm and functional data analysis

Subjects fixated a central point on a screen in the magnet bore while high contrast concentric flickering checkerboard patterns were displayed (visual angle of 39 degrees) via an angulated mirror attached to the RF coil. One run consisted of 36 blocks of 8 seconds stimulation interspersed with 10 to 14 seconds rest totaling a duration of 12: 12 minutes.

Data analysis was performed using BrainVoyager QX 2.8.2 (Brain Innovation, Maastricht, The Netherlands) and custom-written routines in MATLAB. Preprocessing of the fMRI data included 3D rigid body motion correction and temporal high-pass filtering by a GLM with four cosine cycles and linear trend. The data were then co-registered with the structural images using positional information of the acquisitions. Manual adjustments were performed using edge information of the fMRI data. Finally, functional images were resampled in the 3D volume at a resolution of 0.8 mm using sinc interpolation.

A standard GLM was used to assess the functional activation. The visual stimulation regressor was created by convolving the visual activation blocks with a standard 2-gamma-function hemodynamic response function. Each run was analyzed on a single subject level with confound motion regressors (3 translational and 3 rotational).

To produce temporal signal-to-noise ratio (tSNR) maps, preprocessing included only high-pass filtering. No motion correction was applied to avoid additional spatial interpolation. The effect of the visual stimulation was removed from the voxels' time course using a GLM. We then computed tSNR dividing the voxels' temporal mean by the temporal standard deviation.

Results

Phantom measurements

Figure 1 displays the employed RF pulse trains used for the phantom measurements and the corresponding measured and simulated echo signal intensities. Measured data were coil-combined using sum-of-squares. As expected, smaller flip angles are employed in order to sustain the signal longer throughout the echo train. Good agreement between theoretical prediction and experimental results can be observed for all parameter combinations.

Point-spread function simulations and measurements

The results of the simulations and measurements of in-vivo PSF in partition direction are summarized in Table 2. As expected, VFA1 and VFA2 have narrower PSFs than the REF acquisition in both measurements and simulations.

Temporal signal-to-noise ratio

Mean signal and tSNR maps of a representative subject are shown in Figure 2 (all subjects in Supporting Figure 1). The reference acquisition, REF, yields the strongest tSNR; VFA1 and VFA2 have slightly reduced tSNRs. The GRAPPA acquisition, R2, has poor tSNR in comparison to the other acquisitions. All maps reveal reduced tSNR values in the left hemisphere (right side of the image, radiological convention) associated with RF transmission asymmetry. This reduction is more pronounced in the VFA acquisitions.

Functional activation

Maps of functional activation of a representative subject are displayed in Figure 3. All displayed acquisitions, REF (top), VFA1 (middle), and VFA2 (bottom), show robust activation patterns. The strongest activation is confined to regions of gray matter and (in smaller proportion) CSF. The GRAPPA acquisition, R2, is not shown because it revealed very little functional responses. Supporting Figure S2 displays activation maps of all subjects.

To quantify the differences, we calculated within-subject medians of absolute percent signal changes and absolute t-values for all acquisitions using a gray matter mask derived from the anatomical reference data in the mutually covered volume. BOLD signal changes were found to be 14 % (18 %) higher in VFA1 (VFA2) than in REF ($p = 0.02$, uncorr., two-sided Wilcoxon sign rank test). Further, VFA1 and VFA2 did not reveal significantly different t-values than REF. R2 had significantly lower t-values than the other acquisitions ($p < 0.02$), although BOLD signal changes were not significantly different from REF, indicating the same contrast mechanism as in REF but lower tSNR. Individual subject data is provided in supporting Table S1 and Figure S3.

Discussion and Conclusions

We demonstrate the application of variable flip angle refocusing schemes in high resolution 3D-GRASE acquisitions in order to improve the image PSF and spatial coverage in T_2-weighted sub-millimeter fMRI applications at 7 T. In short, the variable flip angle refocusing approach reduces the signal intensity at early echo times and increases it at later echo times. This results in the following: a) Reduced blurring across partitions and/or increased coverage. b) reduced tSNR (in center-out reordering). c) Increased BOLD contrast. We showed that the enhanced BOLD contrast largely counterbalances the reduced tSNR in VFA while image blurring was reduced and therefore conclude that VFA refocusing is a valuable improvement of the single-shot inner-volume 3D-GRASE sequence.

Our method is similar to that of Liang, et al. (34), who recently presented a VFA 3D-GRASE technique for low-resolution whole-brain perfusion measurements using arterial spin labeling at lower field to improve the PSF. Although the scope is different, the employed VFA refocusing RF pulse trains are similar because the ratio of sequence timings and tissue T_2 at 3 T and 7 T are comparable. However, it should be noted that the stronger T_2-weighted stimulated-echo contrast induced by the VFA refocusing has different implications in BOLD imaging than in perfusion imaging, where minimal T_2 contamination is desirable. Further, our study extends the quantitative assessment of the blurring by *direct*, empirical in-vivo measurements of the PSF.

Image point-spread function

Our method was validated using phantom and in vivo measurements. In the phantom scans we noted excellent agreement of simulations and measurements. Compared to conventional refocusing schemes, in-vivo VFA measurements exhibit significantly reduced blurring. With the VFA approach we were able to obtain a similar PSF to that of large FoV 2D SE-EPI along the phase-encoding direction (21). In addition, the coverage of VFA2 was almost doubled compared to REF. REF is in good agreement with (21). Deviations stem from the longer TE and the different fitting approaches. Note that experimental imperfections in the 180° refocusing pulses can be advantageous for the PSF while this is not necessarily the case for lower flip angles. This explains why in REF, the experimental blurring is smaller than theoretically expected. VFA2 exhibits slightly higher blurring than theoretically expected and compared to VFA1. This may be because of physiological noise sources introducing phase shifts throughout the much longer echo train, which could potentially be mitigated using more sophisticated image-reconstruction algorithms (35). Finally, constant flip angle schemes employing angles below 180° (36) would yield a much smaller improvement over 180° pulses than the presented VFA acquisitions. For 140° constant refocusing flip angles we found a reduction of blurring FWHM of 8 % in simulations and 3-8 % in measurements (tested in four subjects), compared to 180° (REF).

tSNR and functional sensitivity

The tSNR in both VFA acquisitions was smaller compared to REF. The reduction was most apparent in regions experiencing insufficient RF transmission (see Figure 2 bottom), to which the VFA acquisitions were more sensitive than the conventional measurement.

Importantly, less RF efficiency, which is typically linked to improved homogeneity (e.g. in B_1 shimming approaches (37,38)), would be acceptable, because of the low SAR of the VFA acquisitions.

Image SNR is commonly known to be dominated by the signal intensity of k-space center (in our case proportional to $\sin^2(\alpha_0)\times\sin^2(\alpha_1/2)$, where α_0 is the excitation flip angle and α_1 the first refocusing angle) and to scale with the square root of the sampling time (depending on the number of slices and partial Fourier acquisition (4)). This explains the reduction of tSNR in VFA1 while the latter partly recovers tSNR in VFA2, because it employs a longer sampling time.

Higher functional signal changes were observed in both VFA acquisitions, thereby preserving the contrast-to-noise ratio and hence functional sensitivity. Higher signal changes are expected because a higher fraction of the sampled signal experiences long echo times (in spin-echo pathways) or long mixing times (in stimulated echo pathways). Thus, in both signal pathways spins experience longer diffusion times in the presence of microscopic magnetic field gradients surrounding capillaries and venules containing deoxygenated blood (dynamic averaging) (1,39,40). This mechanism increases the BOLD contrast. Differential responses from small, adjacent cortical patches or cortical layers can be clouded by image blurring reducing the contrast-to-noise ratio (17,21). The reduced blurring using VFA will therefore improve the functional sensitivity in *differential* functional paradigms (when the areas are aligned with the partition direction of the imaging slab).

Alternative ways to increase FoV

For comparison, in-plane accelerated data were acquired, as an alternative approach to increase the FoV. These did not yield satisfying results. The likely reason is insufficiently distinct RF receive profiles. A different coil design might be advantageous for this application (41), allowing for reduced g-factors. Further, a high resolution receive coil grid with smaller elements might allow for acceleration along the smaller partition direction. Alternatively, independent multi-slab as well as multi-banded (42) multi-slab acquisitions have been demonstrated (43,44). These approaches allow imaging multiples of the FoV in separate locations; however, acquiring an increased, contiguous FoV might be limited by saturation effects from imperfect slab profiles and insufficiently distinct receive RF coil sensitivity profiles, for the separation of the multi-banded slabs in high spatial resolution acquisitions. A larger, contiguous FoV is preferable for applications that focus on imaging larger cortical areas. Note, however, that the VFA technique could straightforwardly be combined with in-plane accelerated imaging and/or these multi-slab approaches.

Supplementary Material

Refer to Web version on PubMed Central for supplementary material.

Acknowledgments

This study was supported by European Research Council (ERC) grant 269853, and the National Institute of Biomedical Imaging and Bioengineering (NIBIB) P41 EB015894. F.D.M. was funded by NWO VIDI (grant 864-13-012).

References

1. Uludag K, Muller-Bierl B, Ugurbil K. An integrative model for neuronal activity-induced signal changes for gradient and spin echo functional imaging. NeuroImage. 2009; 48(1):150–165. [PubMed: 19481163]
2. Duong TQ, Yacoub E, Adriany G, Hu X, Ugurbil K, Kim SG. Microvascular BOLD contribution at 4 and 7 T in the human brain: gradient-echo and spin-echo fMRI with suppression of blood effects. Magnetic resonance in medicine : official journal of the Society of Magnetic Resonance in Medicine / Society of Magnetic Resonance in Medicine. 2003; 49(6):1019–1027.
3. Yacoub E, Van De Moortele PF, Shmuel A, Ugurbil K. Signal and noise characteristics of Hahn SE and GE BOLD fMRI at 7 T in humans. NeuroImage. 2005; 24(3):738–750. [PubMed: 15652309]
4. Edelstein WA, Glover GH, Hardy CJ, Redington RW. The intrinsic signal-to-noise ratio in NMR imaging. Magnetic resonance in medicine : official journal of the Society of Magnetic Resonance in Medicine / Society of Magnetic Resonance in Medicine. 1986; 3(4):604–618.
5. Pohmann R, Speck O, Scheffler K. Signal-to-noise ratio and MR tissue parameters in human brain imaging at 3, 7, and 9.4 tesla using current receive coil arrays. Magnetic resonance in medicine : official journal of the Society of Magnetic Resonance in Medicine / Society of Magnetic Resonance in Medicine. 2015
6. Poser BA, Norris DG. Fast spin echo sequences for BOLD functional MRI. Magma (New York, NY). 2007; 20(1):11–17.
7. Goa PE, Koopmans PJ, Poser BA, Barth M, Norris DG. BOLD fMRI signal characteristics of S1- and S2-SSFP at 7 Tesla. Frontiers in Neuroscience. 2014; 8
8. Barth M, Meyer H, Kannengiesser SA, Polimeni JR, Wald LL, Norris DG. T2-weighted 3D fMRI using S2-SSFP at 7 tesla. Magnetic resonance in medicine : official journal of the Society of Magnetic Resonance in Medicine / Society of Magnetic Resonance in Medicine. 2010; 63(4):1015–1020.
9. Constable RT, Kennan RP, Puce A, McCarthy G, Gore JC. Functional NMR imaging using fast spin echo at 1.5 T. Magnetic resonance in medicine : official journal of the Society of Magnetic Resonance in Medicine / Society of Magnetic Resonance in Medicine. 1994; 31(6):686–690.
10. Hua J, Qin Q, van Zijl PC, Pekar JJ, Jones CK. Whole-brain three-dimensional T2-weighted BOLD functional magnetic resonance imaging at 7 Tesla. Magnetic resonance in medicine : official journal of the Society of Magnetic Resonance in Medicine / Society of Magnetic Resonance in Medicine. 2013
11. Goerke U, Garwood M, Ugurbil K. Functional magnetic resonance imaging using RASER. NeuroImage. 2011; 54(1):350–360. [PubMed: 20699123]
12. Bandettini PA, Wong EC, Jesmanowicz A, Hinks RS, Hyde JS. Spin-Echo and Gradient-Echo Epi of Human Brain Activation Using Bold Contrast - a Comparative-Study at 1.5 T. Nmr Biomed. 1994; 7(1-2):12–20. [PubMed: 8068520]
13. Goense JBM, Logothetis NK. Laminar specificity in monkey V1 using high-resolution SE-fMRI. Magnetic Resonance Imaging. 2006; 24(4):381–392. [PubMed: 16677944]
14. Pfeuffer J, van de Moortele PF, Yacoub E, Shmuel A, Adriany G, Andersen P, Merkle H, Garwood M, Ugurbil K, Hu X. Zoomed Functional Imaging in the Human Brain at 7 Tesla with Simultaneous High Spatial and High Temporal Resolution. NeuroImage. 2002; 17(1):272–286. [PubMed: 12482083]
15. Heidemann RM, Ivanov D, Trampel R, Fasano F, Meyer H, Pfeuffer J, Turner R. Isotropic submillimeter fMRI in the human brain at 7 T: combining reduced field-of-view imaging and partially parallel acquisitions. Magnetic resonance in medicine : official journal of the Society of Magnetic Resonance in Medicine / Society of Magnetic Resonance in Medicine. 2012; 68(5): 1506–1516.
16. Feinberg DA, Hoenninger JC, Crooks LE, Kaufman L, Watts JC, Arakawa M. Inner volume MR imaging: technical concepts and their application. Radiology. 1985; 156(3):743–747. [PubMed: 4023236]
17. Yacoub E, Harel N, Ugurbil K. High-field fMRI unveils orientation columns in humans. Proc Natl Acad Sci U S A. 2008; 105(30):10607–10612. [PubMed: 18641121]

18. Yacoub E, Shmuel A, Logothetis N, Ugurbil K. Robust detection of ocular dominance columns in humans using Hahn Spin Echo BOLD functional MRI at 7 Tesla. NeuroImage. 2007; 37(4):1161–1177. [PubMed: 17702606]
19. Feinberg DA, Oshio K. GRASE (gradient- and spin-echo) MR imaging: a new fast clinical imaging technique. Radiology. 1991; 181(2):597–602. [PubMed: 1924811]
20. Feinberg DA, Harel N, Ramanna S, Ugurbil K, Yacoub E. Sub-millimeter Single-shot 3D GRASE with Inner Volume Selection for T2 weighted fMRI applications at 7 Tesla. 16th Annual Meeting International Society for Magnetic Resonance in Medicine. 2008:2373.
21. Kemper VG, De Martino F, Vu AT, Poser BA, Feinberg DA, Goebel R, Yacoub E. Sub-Millimeter T2 Weighted fMRI at 7 T: Comparison of 3D-GRASE and 2D SE-EPI. Frontiers in Neuroscience. 2015; 9
22. Qin Q. Point spread functions of the T2 decay in k-space trajectories with long echo train. Magn Reson Imaging. 2012; 30(8):1134–1142. [PubMed: 22817958]
23. Hennig J. Multiecho imaging sequences with low refocusing flip angles. Journal of Magnetic Resonance (1969). 1988; 78(3):397–407.
24. Hennig J, Nauerth A, Friedburg H. RARE imaging: a fast imaging method for clinical MR. Magnetic resonance in medicine : official journal of the Society of Magnetic Resonance in Medicine / Society of Magnetic Resonance in Medicine. 1986; 3(6):823–833.
25. Busse RF, Hariharan H, Vu A, Brittain JH. Fast spin echo sequences with very long echo trains: design of variable refocusing flip angle schedules and generation of clinical T2 contrast. Magnetic resonance in medicine : official journal of the Society of Magnetic Resonance in Medicine / Society of Magnetic Resonance in Medicine. 2006; 55(5):1030–1037.
26. Busse RF, Brau AC, Vu A, Michelich CR, Bayram E, Kijowski R, Reeder SB, Rowley HA. Effects of refocusing flip angle modulation and view ordering in 3D fast spin echo. Magnetic resonance in medicine : official journal of the Society of Magnetic Resonance in Medicine / Society of Magnetic Resonance in Medicine. 2008; 60(3):640–649.
27. Griswold MA, Jakob PM, Heidemann RM, Nittka M, Jellus V, Wang J, Kiefer B, Haase A. Generalized autocalibrating partially parallel acquisitions (GRAPPA). Magnetic resonance in medicine : official journal of the Society of Magnetic Resonance in Medicine / Society of Magnetic Resonance in Medicine. 2002; 47(6):1202–1210.
28. Pruessmann KP, Weiger M, Scheidegger MB, Boesiger P. SENSE: sensitivity encoding for fast MRI. Magnetic resonance in medicine. 1999; 42(5):952–962. [PubMed: 10542355]
29. Hennig J, Weigel M, Scheffler K. Multiecho sequences with variable refocusing flip angles: optimization of signal behavior using smooth transitions between pseudo steady states (TRAPS). Magnetic resonance in medicine : official journal of the Society of Magnetic Resonance in Medicine / Society of Magnetic Resonance in Medicine. 2003; 49(3):527–535.
30. Mugler JP 3rd, Epstein FH, Brookeman JR. Shaping the signal response during the approach to steady state in three-dimensional magnetization-prepared rapid gradient-echo imaging using variable flip angles. Magnetic resonance in medicine : official journal of the Society of Magnetic Resonance in Medicine / Society of Magnetic Resonance in Medicine. 1992; 28(2):165–185.
31. Park J, Mugler JP 3rd, Horger W, Kiefer B. Optimized T1-weighted contrast for single-slab 3D turbo spin-echo imaging with long echo trains: application to whole-brain imaging. Magnetic resonance in medicine : official journal of the Society of Magnetic Resonance in Medicine / Society of Magnetic Resonance in Medicine. 2007; 58(5):982–992.
32. Zaitsev M, Hennig J, Speck O. Point spread function mapping with parallel imaging techniques and high acceleration factors: fast, robust, and flexible method for echo-planar imaging distortion correction. Magnetic resonance in medicine : official journal of the Society of Magnetic Resonance in Medicine / Society of Magnetic Resonance in Medicine. 2004; 52(5):1156–1166.
33. Van de Moortele PF, Auerbach EJ, Olman C, Yacoub E, Ugurbil K, Moeller S. T1 weighted brain images at 7 Tesla unbiased for Proton Density, T2* contrast and RF coil receive B1 sensitivity with simultaneous vessel visualization. NeuroImage. 2009; 46(2):432–446. [PubMed: 19233292]
34. Liang X, Connelly A, Tournier JD, Calamante F. A variable flip angle-based method for reducing blurring in 3D GRASE ASL. Physics in medicine and biology. 2014; 59(18):5559–5573. [PubMed: 25170985]

35. Kim H, Kim DH, Park J. Variable-flip-angle single-slab 3D GRASE imaging with phase-independent image reconstruction. Magnetic resonance in medicine : official journal of the Society of Magnetic Resonance in Medicine / Society of Magnetic Resonance in Medicine. 2015; 73(3): 1041–1052.

36. Fernandez-Seara MA, Wang Z, Wang J, Rao HY, Guenther M, Feinberg DA, Detre JA. Continuous arterial spin labeling perfusion measurements using single shot 3D GRASE at 3 T. Magnetic resonance in medicine : official journal of the Society of Magnetic Resonance in Medicine / Society of Magnetic Resonance in Medicine. 2005; 54(5):1241–1247.

37. Metzger GJ, Snyder C, Akgun C, Vaughan T, Ugurbil K, Van de Moortele PF. Local B1+ shimming for prostate imaging with transceiver arrays at 7T based on subject-dependent transmit phase measurements. Magnetic resonance in medicine : official journal of the Society of Magnetic Resonance in Medicine / Society of Magnetic Resonance in Medicine. 2008; 59(2):396–409.

38. De Martino F, Schmitter S, Moerel M, Tian J, Ugurbil K, Formisano E, Yacoub E, van de Moortele PF. Spin echo functional MRI in bilateral auditory cortices at 7 T: An application of B-1 shimming. NeuroImage. 2012; 63(3):1313–1320. [PubMed: 22917678]

39. Yacoub E, Duong TQ, Van De Moortele PF, Lindquist M, Adriany G, Kim SG, Ugurbil K, Hu X. Spin-echo fMRI in humans using high spatial resolutions and high magnetic fields. Magnetic resonance in medicine : official journal of the Society of Magnetic Resonance in Medicine / Society of Magnetic Resonance in Medicine. 2003; 49(4):655–664.

40. Goerke U, van de Moortele PF, Ugurbil K. Enhanced relative BOLD signal changes in T(2)-weighted stimulated echoes. Magnetic resonance in medicine : official journal of the Society of Magnetic Resonance in Medicine / Society of Magnetic Resonance in Medicine. 2007; 58(4):754–762.

41. Koning W, Bluemink JJ, Langenhuizen EA, Raaijmakers AJ, Andreychenko A, van den Berg CA, Luijten PR, Zwanenburg JJ, Klomp DW. High-resolution MRI of the carotid arteries using a leaky waveguide transmitter and a high-density receive array at 7 T. Magnetic resonance in medicine : official journal of the Society of Magnetic Resonance in Medicine / Society of Magnetic Resonance in Medicine. 2013; 69(4):1186–1193.

42. Larkman DJ, Hajnal JV, Herlihy AH, Coutts GA, Young IR, Ehnholm G. Use of multicoil arrays for separation of signal from multiple slices simultaneously excited. Journal of Magnetic Resonance Imaging. 2001; 13(2):313–317. [PubMed: 11169840]

43. Chen, L.; Feinberg, D. Proceedings of the 21st Annual Meeting of ISMRM. Salt Lake City, Utah, USA: 2013. Simultaneous Multi-Volume GRASE Imaging; p. 2365

44. Vu, A.; Feinberg, D.; Harel, N.; Ugurbil, K.; Yacoub, E. Proceedings of the 21st Annual Meeting of ISMRM. Salt Lake City, Utah, USA: 2013. Diagonal multi-slab inner volume 3D GRASE imaging for high resolution T2 weighted fMRI; p. 2364

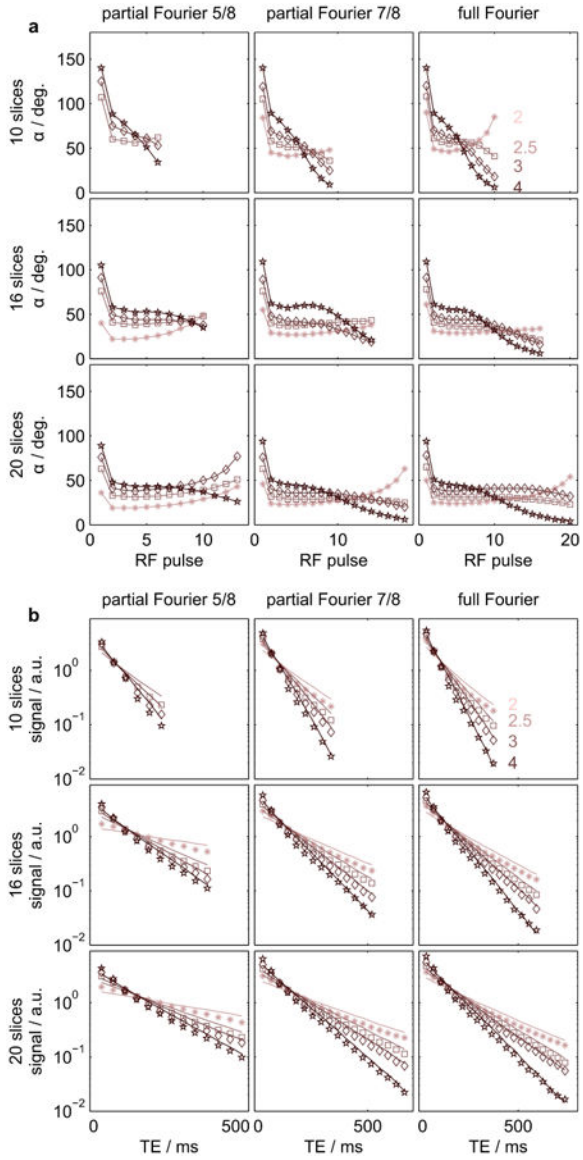

Figure 1.

(**a**) RF pulse flip angles employed in the phantom measurements for different numbers of slices (rows), different partial Fourier factors (columns) and different target PSF FWMH (in pixels, graph colors, annotated in top right graph). (**b**) Corresponding signal intensities. Markers and lines represent experimental data and simulations, respectively. Simulations and experimental data were scaled by their individual means. Size: Double-column width.

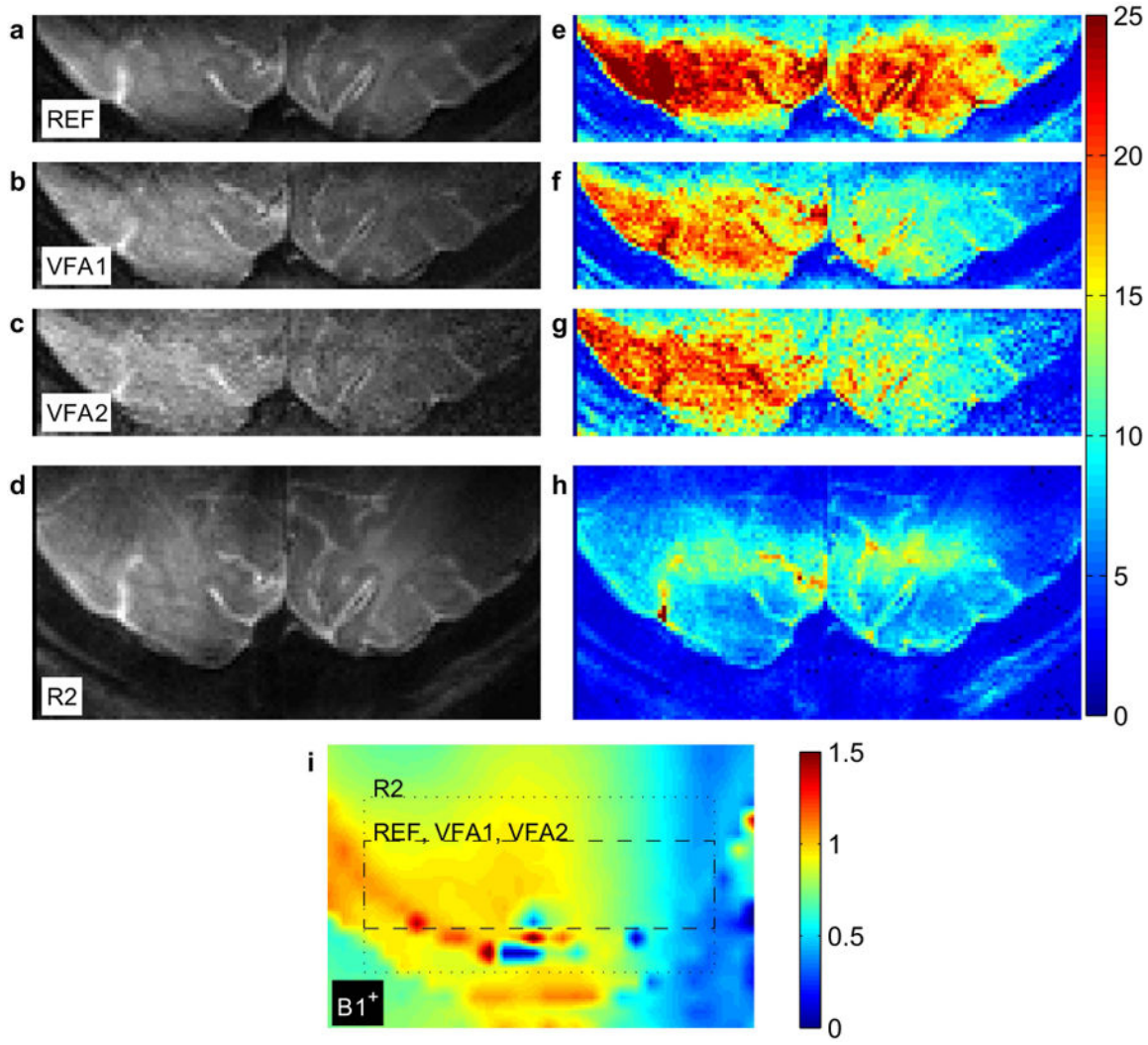

Figure 2.

(**a-d**) Mean signal maps of REF (top), VFA1 (top middle), VFA2 (bottom middle), and R2 (bottom). A single, transversal oblique central slice is shown for each acquisition (identical anatomical position). (**e-h**) Temporal signal to noise ratio maps at position corresponding to maps in a-d. The same color scale is used for all maps. (**i**) Relative RF transmission (B_1^+) map of same location and interpolated to same resolution. The in-plane imaging FoVs of the functional acquisitions are indicated by the dashed (REF, VFA1, VFA2) and dotted (R2) boxes, respectively. Size: Double-column width.

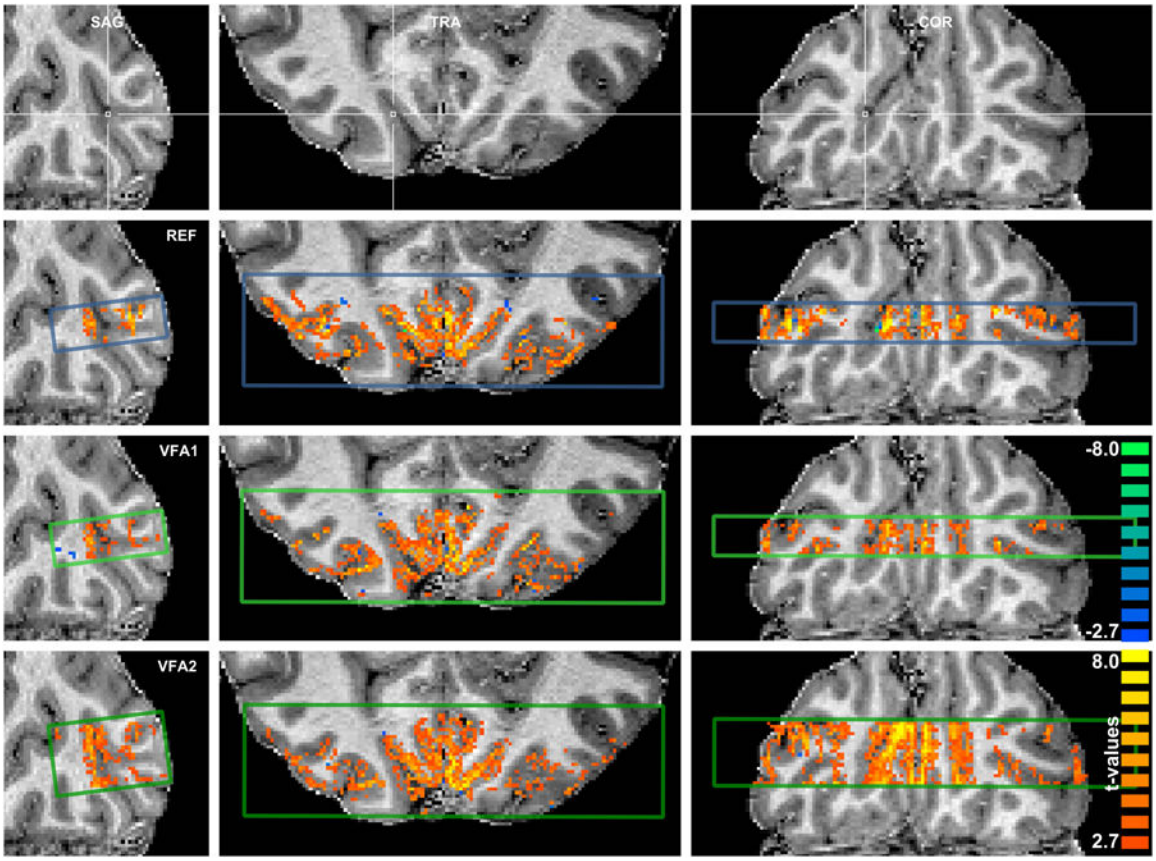

Figure 3.

Visual activation patterns (t-values, two-tailed Student's t-test, $p < 0.01$, uncorrected, 4-voxel cluster-threshold) overlaid on anatomical reference in sagittal, transversal, and coronal cuts. The imaging volume cross section is indicated by the colored boxes in the sagittal cuts and the anatomical reference image at the top (blue: REF, light green: VFA1, dark green: VFA2). Size: Double-column width.

Table 1

Imaging parameters used in in-vivo measurements.

	REF	VFA1	VFA2	R2
TE / TR (ms)	37.9 / 2000	36.9 / 2000	35.9 / 2000	37.9 / 2000
Matrix size	120×30×10	120×30×10	120×30×18	120×60×10
Image volume (mm^3)	96×24×8	96×24×8	96×24×14.4	96×48×8
Turbo factor	6	6	14	6
Echo train duration (ms)	227	221	504	227
Nominal refocusing flip angles	180°	62° to 109°	42° to 90°	180°
Echo-spacing (ms)	1.03	1.03	1.03	1.03

Table 2

FWHM (pixel, mean ± std) of PSF in in-vivo measurements.

Acquisition	Measurement	Simulation
REF	4.0 ± 0.5	4.8
VFA1	2.6 ± 0.3	2.3
VFA2	2.9 ± 0.3	2.3